Supplementary information for

# Low-temperature pseudomorphic transformation of polyhedral MIL-88A to lithium ferrite (LiFe$_3$O$_5$) in aqueous LiOH medium toward high Li storage

Xiaoshi Hu,[a] Shuyan Xiang,[a] Hao Sun,[a] Xiaobing Lou,*[b] Qinqin Xiong,[a] Xiaoxiao Lu,[a] Haiying Qin,[a] Zhenguo Ji[a] and Bingwen Hu[b]

[a]College of Materials & Environmental Engineering, Hangzhou Dianzi University, Hangzhou, 310036, PR China

[b]State Key Laboratory of Precision Spectroscopy, Shanghai Key Laboratory of Magnetic Resonance, Institute of Functional Materials, School of Physics and Materials Science, East China Normal University, Shanghai 200062, P. R. China. E-mail: xiaobinglou@qq.com (X. Lou)

## Table of contents

# A: Experimental section

## 1. Chemicals

The following materials have been used as received from the supplier: Ferric chloride hexahydrate ($FeCl_3 \cdot 6H_2O$, Alfa Aesar, 98%), fumaric acid (Acros, 99%), lithium hydroxide monohydrate ($LiOH \cdot H_2O$, Alfa Aesar, 98%), sodium hydroxide (NaOH, Alfa Aesar, 98%), ethyl alcohol absolute (Sinopharm Chemical Reagent Co., Ltd., 99.7%), and Deionized water (18.2 MΩ cm, Milli-Q, Millipore).

## 2. Preparation of shaped sacrificial MIL-88(A)

For preparation of polyhedral MIL-88(A) preforms, an adapted synthesis from previous work[S1] was carried out: 0.928 g (8 mmol) fumaric acid was first dissolved in 40 mL Milli-Q water under magnetic stirring using a magnetic bar for 1 h at room temperature. Then 1.080 g (4 mmol) of $FeCl_3 \cdot 6H_2O$ was added to the above solution with homogeneous stirring for 30 min. Next, the mixture was placed into a 100 mL Teflon-lined steel autoclave, kept at 100 °C for 12 h before cooling naturally. Large amounts of orange precipitates were recovered for further use by filtration, rising extensively with anhydrous ethyl alcohol and fresh water, and drying in air.

## 3. Pseudomorphic conversion with LiOH

Subsequent pseudomorphic transformation of so prepared solid body MIL-88(A) was performed to yield targeted monolithium ferrite-based replicate at gram level. 0.514 g of the MIL-88(A) preform powders were soaking in a concentrated LiOH solution (40mL, 1.6 M) and heated in the air-flow electric oven at 170 °C for 24 h. After the reaction was complete, the supernatant liquid of the reaction mixture is discarded, and the resulting maroon crystals were collected and washed by water and ethanol and finally dried at 80 °C.

## 4. Apparatus

The crystal information of the sample was investigated by XRD (Holland PANalytical PRO PW3040/60 diffractometer) using Cu Kα radiation (λ = 1.5418 Å). Thermal behaviors of the samples were investigated using STA 449 F3 Jupiter® simultaneous thermal analyzer in air up to 800 °C at a heating rate of 10 °C min$^{-1}$. The morphologies and (micro)structures of as-prepared materials were analyzed by FESEM (Hitachi S-4800) and (HR)TEM (FEI Tecnai F20). The amounts of lithium and iron in the reaction products were analyzed by atomic absorption and inductively coupled plasma optical emission spectrometry (ICP-OES, Agilent ICP-OES 720). Nitrogen sorption measurements were performed on a Micromeritics analyzer (TriStar II 2460) at 77 K. The samples were degassed at 100 °C for 12 h. XPS measurements was conducted on a Thermo ESCALAB 250XI system with a monochromatic Al Kα source (1486.6 eV). The C 1s peaks were corrected to 284.6 eV, and all the other peaks were normalized accordingly. Varian 700 M was used to collect $^1$H-NMR data in liquid state. For ex-situ PXRD and XPS tests, the cycled electrodes were disassembled in an Ar-filled glovebox, rinsed with anhydrous dimethyl carbonate, dried naturally in the argon-filled glovebox for a few hours, and then transferred directly to the PXRD or XPS sample chamber. MAS NMR experiments were performed on a wide-bore 14.1 T Bruker Advance

III spectrometer operating at Larmor frequencies of 233.23 MHz for $^7$Li. A Triple-resonance 2.5 mm MAS probe was used for spinning the packed rotors at 20 kHz. The $^7$Li MAS NMR spectra were acquired using Hahn echo pulse sequence with a recycle delay of 0.1 s and 20000 scans. The carrier frequency was set to -1000, 1000, and 3000 ppm, respectively and the spectral width was set to ~3600 ppm. All the spectra were referenced to aqueous LiCl soltuion.

## 5. Electrochemical measurements

Test cells (2032 coin-type half cells) were assembled inside the Ar-filled glovebox with $O_2$ and $H_2O$ contents below 0.5 ppm. In the cell assembly, Li metal was used as the counter/reference electrode, Cu current collector carrying active material ($LiFe_3O_5$) as the working electrode, Celgard 2325 as a separator, and 1 M lithium hexafluorophosphate ($LiPF_6$) dissolved in solvent mixture of ethylene carbonate (EC)/ethyl methyl carbonate (EMC)/dimethyl carbonate (DMC) (1/1/1 vol%) with 5% fluoroethylene carbonate (FEC) as the electrolyte. The working electrodes were prepared with a conventional slurry coating method. 70 wt% $LiFe_3O_5$, 20 wt% Super-P carbon black and 10 wt% sodium carboxymethyl cellulose (CMC) in water were mixed to form a homogenous slurry. Then the slurry was uniformly spread onto Cu foil substrate and dried at 100 °C in vacuum overnight. The dried electrode was cast into a disk of 14 mm in diameter for assembling cells, with average active substance mass loading around 1.5 mg. Charging/discharging tests of the cells were performed on a multichannel battery tester (LAND CT2001A) between 0.01 and 3.00 V versus Li/Li$^+$ at room temperature. CVs were measured on an electrochemical workstation (Autolab PGSTAT302N) and EIS in the frequency range of 100 kHz to 0.1 Hz at room temperature. All of the electrochemical cell tests were carried out after aging for 24 h of the fresh cells.
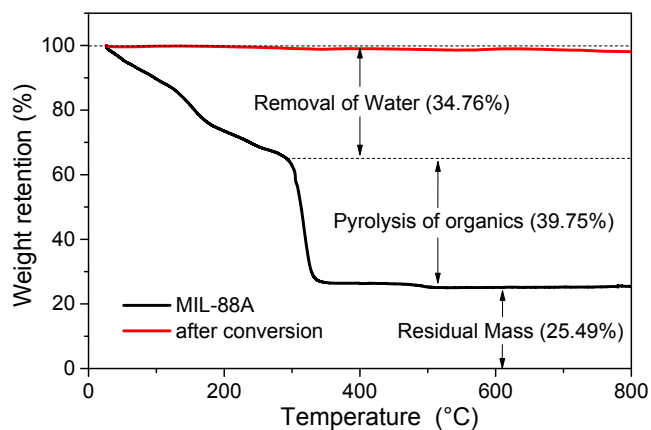
# B: Supplementary figures



**Fig. S1** TG curve of samples of as-prepared (hydrated) MIL-88A crystals before (black) and after (red) conversion.
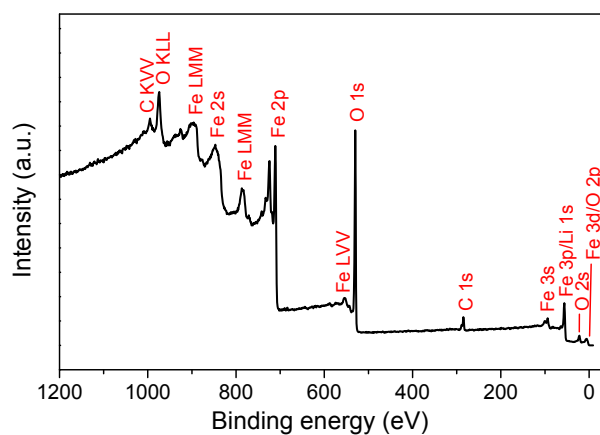


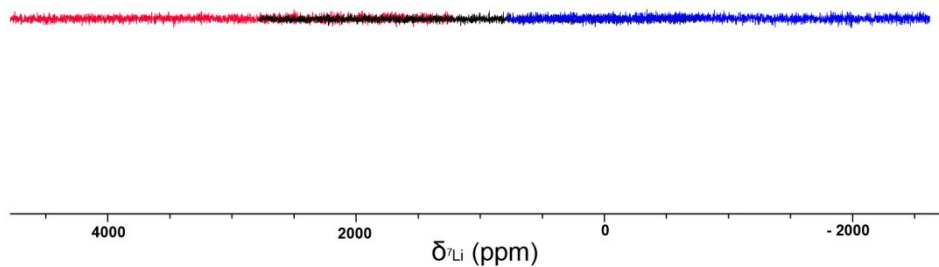**Fig. S2** Full survey XPS spectrum of the as-obtained $LiFe_3O_5$ product



**Fig. S3** $^7Li$ NMR spectra of the as-obtained $LiFe_3O_5$ product. Spectra were recorded with varied offset, which is indicated by the color.
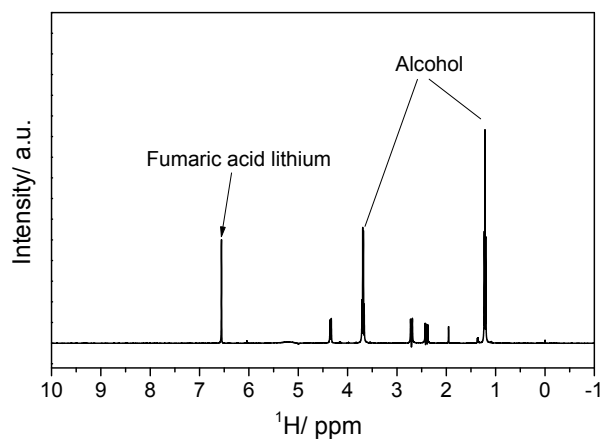
**Fig. S4** $^1$H-NMR spectrum recorded in D$_2$O for the clear solution gathered after digestion of MIL-88A in the basic media. The proton signals are well assigned to the FMA molecule (fumarate dianions). The faint signals are from the impurities in the solvent.
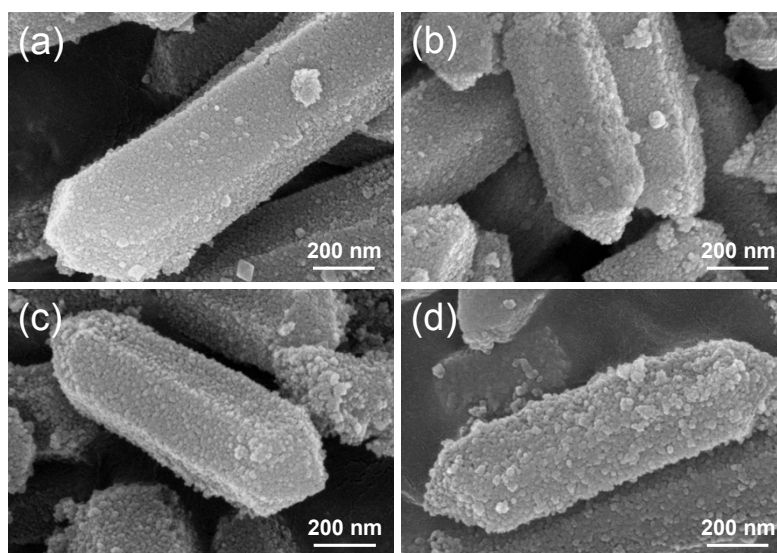


**Fig. S5** High-magnification SEM micrograph taken at (a) 2 min, (b) 10 min, (c) 30 min, and (d) 12h during solution mediated transformations of MIL-88A.
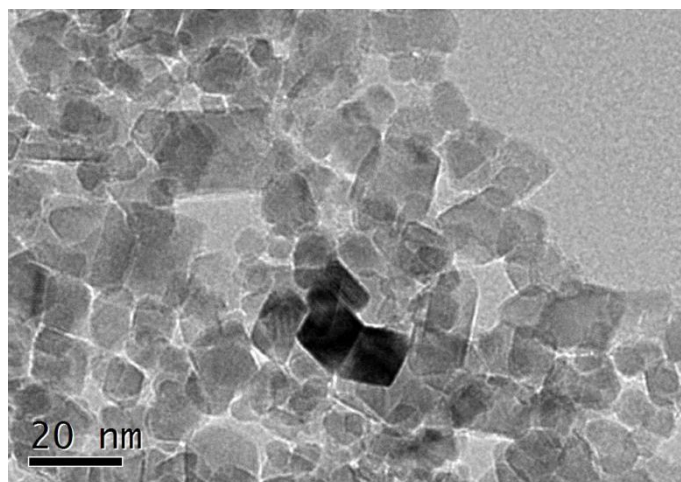
**Fig. S6** High-magnification TEM image showing interstitial pores between the LiFe$_3$O$_5$ nanocrystal.
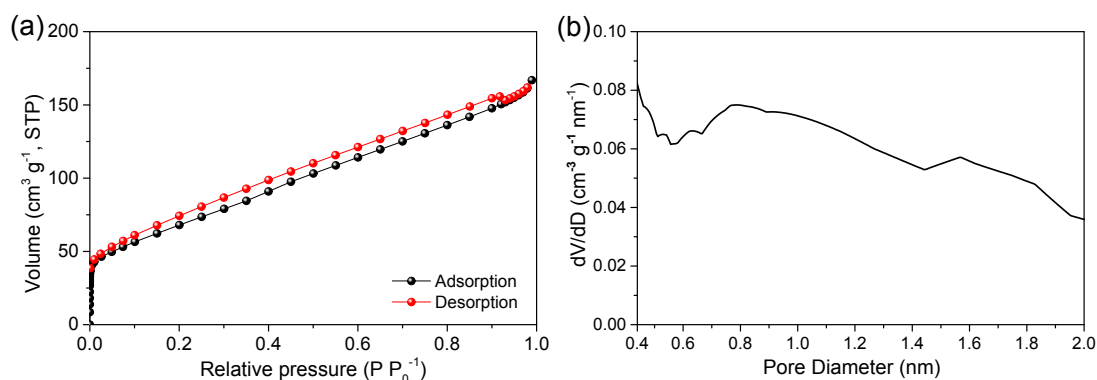


**Fig. S7** (a) N$_2$ adsorption/desorption isotherms and (b) corresponding micropore size distribution for original MIL-88A. The gas adsorption follows type I isotherms, that conforms to its intrinsic microporosity, as can also be revealed by the measured narrow pore size of a few angstroms. Sorption experiments of MIL-88A gave a micropore volume of 0.155 cm$^3$ g$^{-1}$ (HK method), which is similar to previous results.[S2,19]
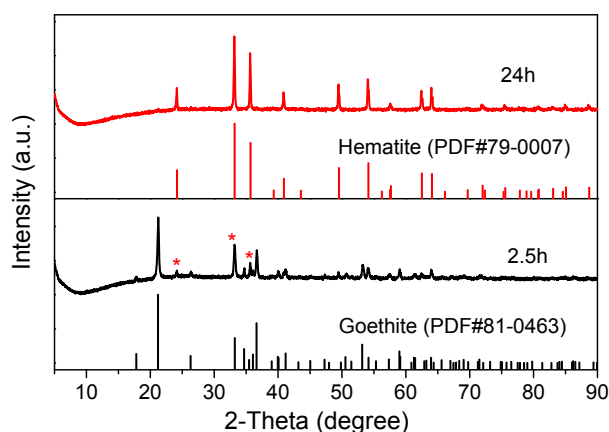


**Fig. S8** Experimental XRD patterns recorded at different time intervals (as indicated) during solution mediated transformations of MIL-88A in 1.6 M NaOH at 170 °C; patterns simulated from structural data of α-Fe$_2$O$_3$ (hematite, red bars) and α-FeOOH (goethite, dark gray bars) are presented for comparison; the red asterisks indicate reflections that belong to α-Fe$_2$O$_3$.
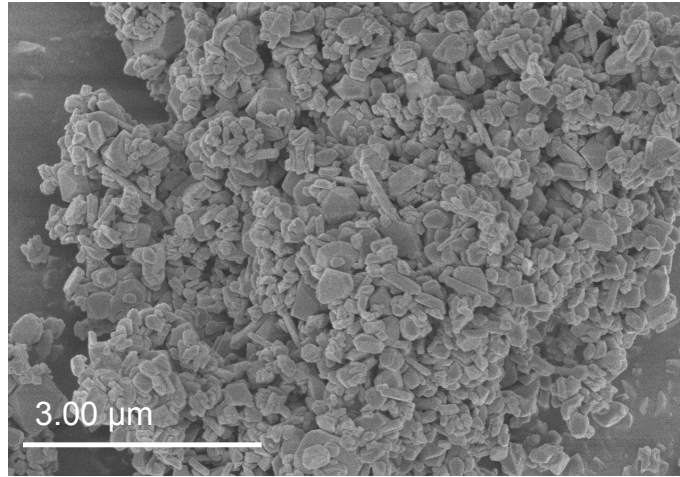
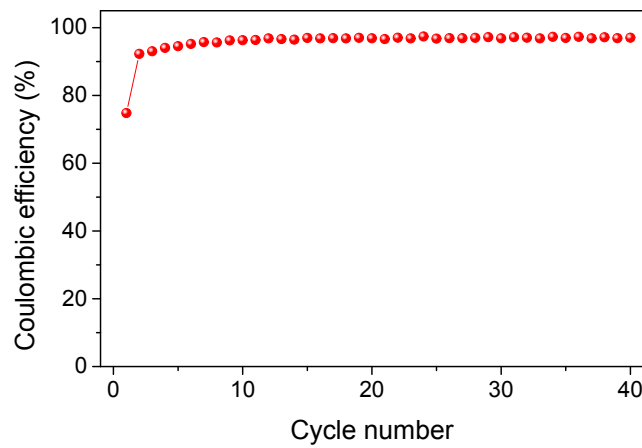**Fig. S9** SEM micrograph of the product formed in NaOH medium.



**Fig. S10** CE of lithium ferrite anode when cycling at 0.1 A g$^{-1}$.
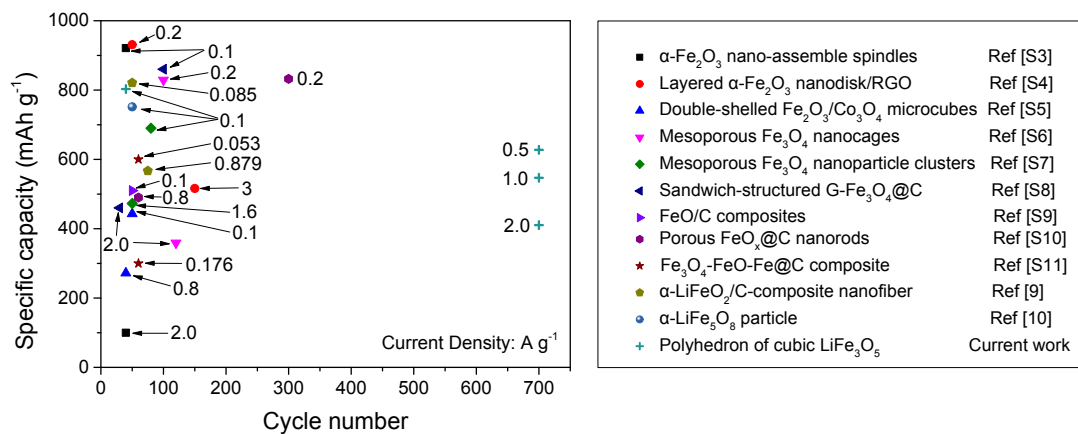


**Fig. S11** Relationship between the specific capacity and cycle performance of recently reported iron-based anode materials (inset shows current rates and reference number).[S3-11,9,10]
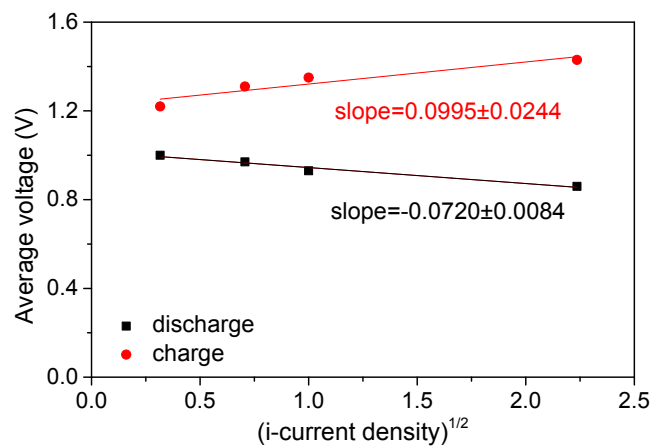
**Fig. S12** Linear fit of the average voltage vs. the square root of the current density of lithium ferrite electrode.
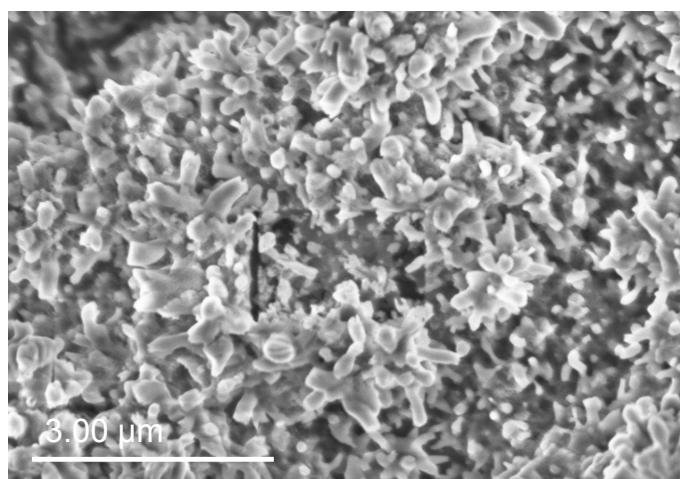


**Fig. S13** SEM micrograph of lithium ferrite electrode at charged state after 400 cycles at 0.5 A g$^{-1}$.

## Supplementary references

S1.     P. Horcajada, T. Chalati, C. Serre, B. Gillet, C. Sebrie, T. Baati, J. F. Eubank, D. Heurtaux, P. Clayette, C. Kreuz, J.-S. Chang, Y. K. Hwang, V. Marsaud, P.-N. Bories, L. Cynober, S. Gil, G. Férey, P. Couvreur and R. Gref, *Nat. Mater.*, 2009, **9**, 172.

S2.     J. Amaro-Gahete, R. Klee, D. Esquivel, J. R. Ruiz, C. Jiménez-Sanchidrián and F. J. Romero-Salguero, *Ultrason. Sonochem.*, 2019, **50**, 59-66.

S3.     A. Banerjee, V. Aravindan, S. Bhatnagar, D. Mhamane, S. Madhavi and S. Ogale, *Nano Energy*, 2013, **2**, 890-896.

S4.     J. Qu, Y.-X. Yin, Y.-Q. Wang, Y. Yan, Y.-G. Guo and W.-G. Song, *ACS Appl. Mater. Interfaces*, 2013, **5**, 3932-3936.

S5.     Z. Li, B. Li, L. Yin and Y. Qi, *ACS Appl. Mater. Interfaces*, 2014, **6**, 8098-8107.

S6.     T. Xia, X. Xu, J. Wang, C. Xu, F. Meng, Z. Shi, J. Lian and J.-M. Bassat, *Electrochim. Acta*, 2015, **160**, 114-122.

S7.     S. H. Lee, S.-H. Yu, J. E. Lee, A. Jin, D. J. Lee, N. Lee, H. Jo, K. Shin, T.-Y. Ahn, Y.-W. Kim, H. Choe, Y.-E. Sung and T. Hyeon, *Nano Lett.*, 2013, **13**, 4249-4256.

S8.     L. Zhao, M. Gao, W. Yue, Y. Jiang, Y. Wang, Y. Ren and F. Hu, *ACS Appl. Mater. Interfaces*, 2015, **7**, 9709-9715.

S9.     M. Gao, P. Zhou, P. Wang, J. Wang, C. Liang, J. Zhang and Y. Liu, *J. Alloys Compd.*, 2013, **565**, 97-103.

S10.    X. Li, Z. Zhang, J. Li, Y. Ma and Y. Qu, *J. Mater. Chem. A*, 2015, **3**, 18649-18656.

S11.    X. Zhao, D. Xia and K. Zheng, *J. Alloys Compd.*, 2012, **513**, 460-465.